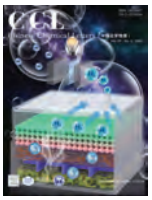
Chinese Chemical Letters 37 (2026) 111171

Contents lists available at ScienceDirect

Chinese Chemical Letters

journal homepage: www.elsevier.com/locate/cclet



Orthogonal configurative dye 2-anthryl asymmetric aza-BODIPY enhancing SOCT-ISC for phototherapy

Shu Lv[a,1], Xiuyan Gong[b,1], Yunsheng Xue[c], Gaowu Qin[a,*], Xin-Dong Jiang[a,*], Guiling Wang[b,*]

[a] Institute for Strategic Materials and Components, Liaoning & Shenyang Key Laboratory of Functional Dye and Pigment, Shenyang University of Chemical Technology, Shenyang 110142, China
[b] Key Laboratory of Cell Biology, Department of Cell Biology, School of Life Sciences, China Medical University, Shenyang 110122, China
[c] Jiangsu Key Laboratory of New Drug Research and Clinical Pharmacy, School of Pharmacy, Xuzhou Medical University, Xuzhou 221004, China

ARTICLE INFO

Article history:
Received 6 January 2025
Revised 26 March 2025
Accepted 1 April 2025
Available online 2 April 2025

Keywords:
Anthracene
Heavy-atom-free
Aza-BODIPY
ROS
Orthogonal configuration

ABSTRACT

Orthogonal molecular orbitals (MOs) of donor-acceptor (D-A) pairs favor the spin-orbit charge transfer intersystem crossing (SOCT-ISC) transition, and herein 2-anthryl asymmetric aza-boradiazaindacene (aza-BODIPY) (AH-BDP) was designed and prepared. According to the X-ray crystallography, the steric hindrance in orthogonal molecule AH-BDP results in a large dihedral angle between the two MO planes. Since low ΔE_{st} prefers to undertake ISC and efficiently produce reactive oxygen species (ROS), the calculated ΔE_{st} for AH-BDP is 0.757 eV, significantly smaller than that of the aza-BDOPY without anthryl group DH-BDP (1.052 eV). AH-BDP as a heavy-atom-free photosensitizer not only produced the singlet oxygen, but also possessed photothermal conversion efficiency. Self-assembly AH-BDP nanoparticles (NPs) could efficiently induce HCT116 cells elimination in nude mice through ROS/heat-mediated pathways.

© 2026 Published by Elsevier B.V. on behalf of Chinese Chemical Society and Institute of Materia Medica, Chinese Academy of Medical Sciences.

As the incidence of cancer continues to rise annually, the development of efficient and safe cancer treatment becomes an urgent issue. Compared to traditional treatment approaches, phototherapy, such as photothermal therapy (PTT) or photodynamic therapy (PDT), has garnered significant attention due to their non-invasive nature and minimal side effects [1–3]. PTT employs photothermal agent that converts light into heat through non-radiative decay when exposed to the laser of specific wavelength, enabling localized thermal treatment of cancerous tissues [4–7]. In contrast, PDT utilizes photosensitizer (PS) to yield superoxide anion/hydroxyl radicals and singlet oxygen *via* electron transfer (type I reaction) and energy transfer (type II reaction) processes, respectively [8–10]. These reactive oxygen species (ROS) could effectively kill cancer cells [11].

Phototherapy agent plays a crucial role in PTT/PDT, leading to a sustained increase for developing and designing novel structures. Among them, aza-boradiazaindacene (aza-BODIPY) has attracted considerable interest due to its long-wavelength, high molar extinction coefficient and ease of modification [12–18]. Indeed, introduction of some heavy atoms (Br, I) into aza-BODIPY, can effectively enhance the intersystem crossing (ISC) and facilitate the generation of ROS for PDT [19–23]. However, the heavy atom also poses potential dark toxicity [24–26], which could compromise the safety of cancer treatment, thus and heavy-atom-free aza-BODIPY presents a promising avenue for further research [27,28].

The spin-orbit charge transfer intersystem crossing (SOCT-ISC) is found to effectively solve the above problem [29–31]. Orthogonal molecules with light excitation undergo charge separation and recombinated processes, overcoming the limitations associated with traditional heavy atom approaches [32]. Since the orthogonal molecular orbitals (MOs) of donor-acceptor (D-A) pairs favor the SOCT-ISC transition, BODIPY with the anthryl group at *meso* site was popularly designed, owing to steric hindrance to produce a large dihedral angle between the two MO planes. According to the X-ray crystallography, indeed the orthogonal structure between the anthryl group at *meso* site and the parent nucleus BODIPY was confirmed by Yang *et al.* [33]. Subsequently, Sun *et al.* reported heavy-atom-free nanomaterials based on aza-BODIPY, which promotes ISC by SOCT to produce ROS, and acts as storage for the reversible capture and release of ROS to enhance PDT efficacy [34]. Very recently, our group prepared dye with 1,7-di-anthryl groups in aza-BODIPY system for the first time, owing to steric hindrance to produce a large dihedral angle between the two MO planes [35].

* Corresponding authors.
E-mail addresses: gwqin@syuct.edu.cn (G. Qin), xdjiang@syuct.edu.cn (X.-D. Jiang), glingwang@cmu.edu.cn (G. Wang).
[1] These authors contributed equally to this work.

https://doi.org/10.1016/j.cclet.2025.111171
1001-8417/© 2026 Published by Elsevier B.V. on behalf of Chinese Chemical Society and Institute of Materia Medica, Chinese Academy of Medical Sciences.

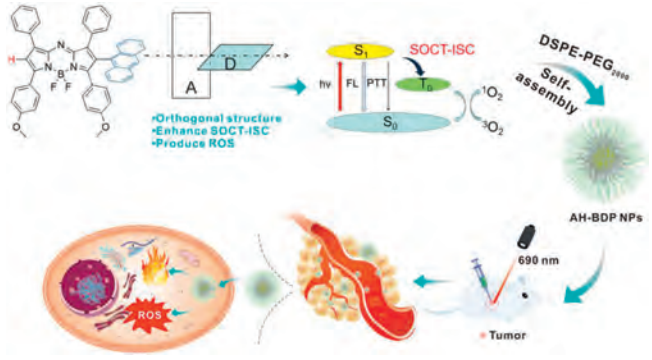
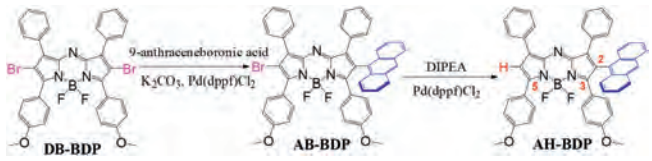


Fig. 1. Design strategies for AH-BDP with 2-anthryl groups in aza-BODIPY system, preparation of self-assembled AH-BDP NPs, and theranostic mechanisms.



Scheme 1. Synthesis of AH-BDP with anthryl group at 2-site in aza-BODIPY.

Indeed, anthracene as a heavy-atom-free group embedded in aza-BODIPY can form an orthogonal structure that improves the generation of ROS [35]. Therefore, based on the unique aza-BODIPY core and the significant steric hindrance of anthracene, we herein introduced an anthryl group to aza-BODIPY at 2-site (Fig. 1), confirming an orthogonal structure by X-ray crystal for the first time. This orthogonal molecule AH-BDP, as a heavy-atom-free PS, can effectively produce ROS, and also possess the photothermal conversion effect. According to PTT/PDT co-therapy, self-assembly AH-BDP nanoparticles (NPs) can efficiently induce cancer cell elimination through ROS/heat-mediated pathways.

Using 2,6-dibromo DB-BDP as the starting material [36], we performed a Suzuki coupling reaction to introduce mono-anthryl moiety to aza-BODIPY (AB-BDP) [37,38]. Then, the mono-anthryl AH-BDP was successfully prepared by the reaction of AB-BDP with *N*,*N*-diisopropylethylamine (DIPEA)/Pd(dppf)Cl_2, achieving a yield of 30 % (Scheme 1). Moreover, the structures of aza-BODIPYs AB-BDP (CCDC: 24100364) (Fig. S1a in Supporting information) and AH-BDP (CCDC: 24100365) were unequivocally confirmed by X-ray analysis (Fig. 2a), which show that all the structures have slightly distorted sp^3 geometry for the boron atom. We found that the steric bulk of the anthryl group was forced to adopt a *pseudo*-orthogonal structure, avoiding the stereo repulsion (Fig. 2b and Fig. S1b in Supporting information). The dihedral angle between the anthryl group and the nucleus in AH-BDP is 70.6° (Fig. 2b), approaching the ideal value of 90°. Especially, for BA-BDP the corresponding dihedral angle (87.8°) is even nearer to 90° (Fig. S1b).

In terms of spectral properties, the maximum absorption of AH-BDP exhibited a bathochromic shift to 680 nm in the NIR region (Table S1 in Supporting information), compared to those of DB-BDP (λ_{abs} = 676 nm) and AB-BDP (λ_{abs} = 676 nm) in CH_2Cl_2 (Fig. S2a and Table S2 in Supporting information). This confirmed that the introduction of the anthryl moiety at 2-site could slightly lead to bathochromic shift of the absorption maxima. Additionally, we measured the absorption spectra of AH-BDP in various solvents. All absorption maxima fell within the narrow region of 672–688 nm (Fig. 2c and Table S1), and emission maxima are in the relatively wide range of 708–740 nm (Fig. 2d). Especially, the fluorescence quantum yield of AH-BDP (Φ_f = 30 % in CH_2Cl_2) is higher than that (2 %) of AB-BDP, due to the heavy-atom effect. In addition, the dual

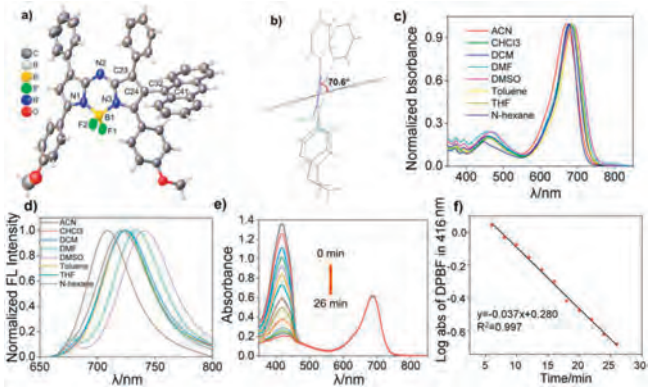


Fig. 2. (a) Oak Ridge thermal ellipsoid plot (ORTEP) views of AH-BDP (CCDC: 24100365) (displacement ellipsoids at the 30 % probability level). (b) Side views of the molecular structure. Selected angles (°): C23-C24-C32-C41, 70.6 (5). (c) Normalized absorption and (d) emission spectra of AH-BDP in various organic solutions at 298 K. (e) Time-dependent photo degradation of DPBF with AH-BDP. (f) DPBF degradation rate curves with AH-BDP in toluene.

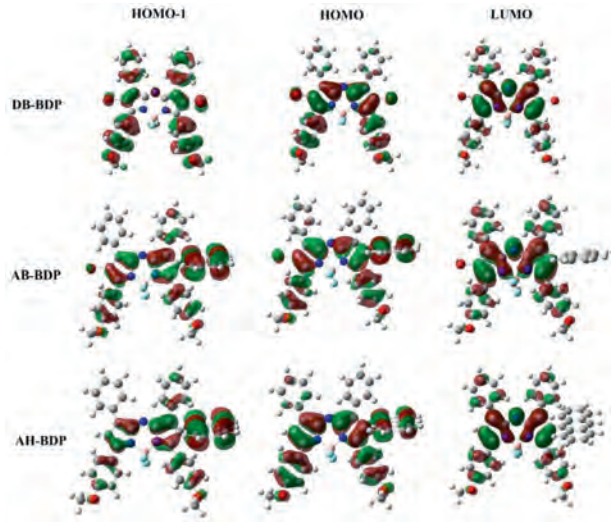


Fig. 3. Frontier MO profiles and energies (eV) of the studied species. ΔE_1 = LUMO-HOMO. ΔE_2 = LUMO-HOMO-1.

absorption bands of the anthryl moiety in AH-BDP were observed to be 372 and 392 nm (Fig. 2c).

To gain insight into the photophysical and electronic properties of the studied systems, the theoretical calculations were performed to obtain the spectral properties and the frontier MO distribution. Table S3 (Supporting information) gives the calculated maximum absorption wavelength, oscillator strength, and the assignment of main absorption peaks at the PCM-D3(BJ)-B3LYP/6-311+G(d) level. The frontier MO distribution is presented in Fig. 3. It can be seen from Table S3 that the calculated $\lambda_{max,abs}$ are in line with the corresponding experimental values. The main absorption peaks of the studied systems mainly correspond to the electronic transitions from highest occupied molecular orbital (HOMO) and HOMO-1 to lowest unoccupied molecular orbital (LUMO). As shown in Fig. S3 (Supporting information), the HOMO and HOMO-1 orbitals of DB-BDP are mainly distributed on the pyrrole rings and the phenyl rings at 3,5-sites (Scheme 1), while the LUMO is mainly centered on the aza-BODIPY moiety. Similar is for the cases of AB-BDP and AH-BDP, where the electron density is further distributed on the anthryl moiety at 2-site for the HOMO and HOMO-1 orbitals. The electronic transition responsible for the maximum absorption wavelength presents intramolecular charge transfer (ICT) charac-

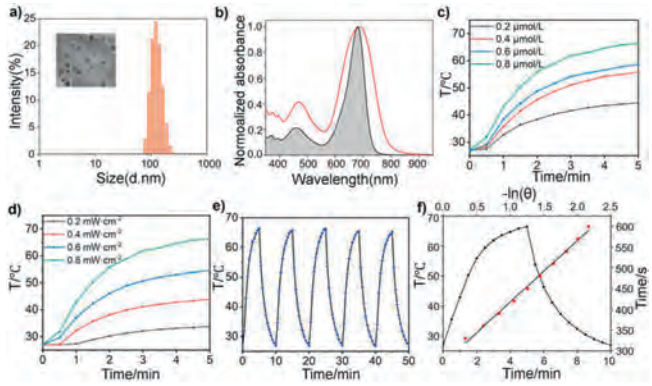


Fig. 4. (a) DLS of AH-BDP NPs in aqueous solution. Inset image: TEM of AH-BDP NPs. Scale bar: 200 μm. (b) Absorption of AH-BDP (black curve) in CH_2Cl_2 and AH-BDP NPs (red curve) in aqueous solution. (c) Temperature changes of AH-BDP NPs at different concentrations (20−80 μmol/L) under 690 nm laser irradiation (0.8 W/cm^2). (d) Photothermal conversion of AH-BDP NPs (80 μmol/L) under 690 nm laser irradiation with different power density (0.2−0.8 W/cm^2). (e) Photothermal stability study during five circles of heating-cooling processes. (f) Temperature response curves of AH-BDP NPs in aqueous solutions under irradiation and naturally cooling, and Linear fitting of –ln(θ) and time.

teristics. From the results of the energy gap between HOMO and LUMO (ΔE_1), AH-BDP presents a smaller ΔE_1 (2.01 eV) than that of DB-BDP (2.05 eV) and AB-BDP (2.13 eV). This implies a redshift of the absorption maxima with the introduction of anthryl moiety at 2-site, which explains the experimental observations. Additionally, the S2 state is ascribed to exciting an electron from HOMO-1 to LUMO (ΔE_2), and the lower energy gap (ΔE_2) in AH-BDP corresponds to the absorption peak at 459 nm in CH_2Cl_2 (Fig. 2c).

To investigate ROS generation capability, monochromatic light at 690 nm was employed to irradiate AH-BDP in toluene, with 1,3-diphenylisobenzofuran (DPBF) serving as the singlet oxygen ($^1O_2$) indicator [39–42]. The efficiency of $^1O_2$ generation was evaluated by monitoring the decrease in absorbance of DPBF at 416 nm, using methylene blue (MB, $\Phi_\Delta = 0.57$ in dichloromethane (DCM) as a reference [43]. Based on the linear relationship observed in the decay curves (S = −0.037), the $^1O_2$ yield of AH-BDP was calculated to be 0.15 (Figs. 2e and f). Indeed, due to the orthogonal structure enhancing SOCT-ISC, the singlet oxygen is generated by AH-BDP with irradiation, compared to that ($\Phi_\Delta = 0.02$) of aza-BDOPY without anthryl group DH-BDP (Table S4 in Supporting information). Furthermore, utilizing dihydrorhodamine 123 (DHR123) as an indicator, we explored whether AH-BDP could produce type I ROS under irradiation. DHR123 showed a negligible change in fluorescence intensity when AH-BDP were illuminated in DMSO solution (Fig. S4 in Supporting information), suggesting that no type I ROS was produced. To further understand the mechanism of $^1O_2$ generation, we calculated the energy gap of S_1-T_1 (ΔE_{st}), which is an important indicator of the ISC efficiency. Low ΔE_{st} prefers to undertake ISC and efficiently produce $^1O_2$ [28]. The calculated ΔE_{st} for AH-BDP is 0.757 eV, significantly smaller than that of the aza-BDOPY without anthryl group DH-BDP (1.052 eV) (Table S4). This implies that AH-BDP may possess higher ISC efficiency and thus generate ROS more efficiently, in agreement with the experimental results.

To enhance the biocompatibility and water solubility of AH-BDP, we encapsulated it with 1,2-distearoyl-*sn*-glycero-3-phosphoethanolamine-*N*-[hydroxy(polyethyleneglycol)-2000] ($DSPE\text{-}PEG_{2000}$) to give AH-BDP NPs [44–46]. Dynamic light scattering (DLS) measurements indicated a suitable hydrodynamic diameter ranging from 70 nm to 200 nm (Fig. 4a), and the average hydrodynamic diameter and the polydispersity index (PDI) were 114.7 nm and 0.285 (Fig. 4a). Furthermore, the morphology of AH-BDP NPs was examined using transmission electron microscopy (TEM). The results showed that AH-BDP NPs were stable enough to adopt a near-spherical shape after dispersion in water (Figs. S5 and S6 in Supporting information). In addition, the absorption spectrum ($\lambda_{abs} = 688$ nm) of AH-azaBDP NPs in aqueous solution became wider, comparing to that ($\lambda_{abs} = 680$ nm) of AH-azaBDP in CH_2Cl_2 (Fig. 4b).

Next, to verify whether the introduction of the anthryl moiety affects the photothermal properties of aza-BODIPY (Fig. S7 in Supporting information), we investigated the photothermal conversion efficiencies (PCE) of AH-BDP NPs. We monitored the temperature changes of aqueous solution in presence/absence of AH-BDP NPs under irradiation. We found that, the temperature change of the aqueous solution in the absence of AH-BDP NPs can be ignored under continuous illumination. On the contrary, in the presence of AH-BDP NPs, the temperature of the aqueous solution undergoes a dramatic change, indicating that AH-BDP NPs have a good photothermal conversion effect. Using a laser at 0.8 W/cm^2 and irradiating with monochromatic light at 690 nm, the temperature of aqueous solution increased by 40 °C after 5 min (Fig. 4c). We also measured the temperature changes at various light intensities (0.2–0.8 W/cm^2) (Fig. 4d). The photothermal effect was found to increase with both concentration and light intensity. After undergoing five cycles, the temperature continued to rise by 40 °C, confirming the good stability of AH-BDP NPs in water (Fig. 4e). The photothermal conversion efficiency (PCE, η) was calculated based on one cycle of the heat-cooling process (Fig. 4f). It was found that the PCE of AH-BDP NPs was 54 %, and much higher than ICG ($\eta \approx$ 3.1 %) [47].

Considering the singlet oxygen generation and photothermal conversion, AH-BDP NPs are preferred as the reagent for *in vitro* and *in vivo* experiments. First, human colon cancer cells (HCT116) were treated with varying concentrations of AH-BDP NPs (0–40 μmol/L) to assess its concentration-dependent effects under 690 nm laser irradiation. The results demonstrated that AH-BDP NPs in combination with laser irradiation significantly reduced cell viability compared to the control, AH-BDP NPs-only, and laser-only groups (Fig. 5a). To further investigate how AH-BDP NPs influences cancer cell survival under laser irradiation, we employed a calcein-AM/propidium iodide (PI) dual-staining assay. This method stains live cells green and dead cells red. As shown in Fig. 5b, the combined AH-BDP NPs and laser treatment caused extensive damage to HCT116 cells, as evidenced by prominent red fluorescence. In contrast, the control, laser-only, and AH-BDP NPs-only groups displayed strong green fluorescence, indicating minimal cell damage in these groups. Flow cytometry was then performed to evaluate the apoptosis-inducing potential of AH-BDP NPs. The results revealed a substantial increase in apoptotic and necrotic cells in AH-BDP NPs combined with laser group compared to the single-treatment groups. These findings confirmed that the combination of AH-BDP NPs and laser irradiation effectively induces cell death in HCT116 cells (Fig. 5c).

Since ROS are closely linked to tumorigenesis and apoptosis, we measured ROS levels in all experimental groups using a ROS detection kit (Fig. 5d). The AH-BDP NPs combined with laser group exhibited the highest ROS generation, indicating that this treatment disrupted oxidative homeostasis and caused significant damage to cancer cells (Fig. 5d). To examine the *in vivo* effects, we conducted a tumor formation experiment in nude mice (Fig. 5e). The animal experiments conducted in this article have been approved by the Animal Center of China Medical University (approval number CMU20241627). The drug and irradiation combination group displayed the strongest tumor suppression compared to other groups (Fig. 5f), with significantly lower tumor weights and volumes (Figs. 5g and h). So, these results demonstrate that the combination of AH-BDP NPs and laser irradiation effectively induces cancer cell

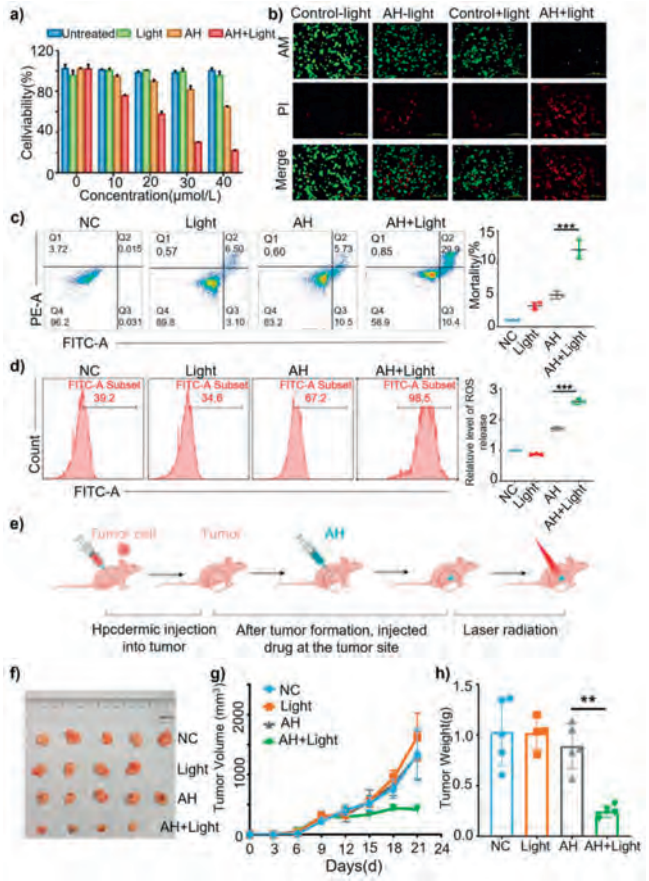


Fig. 5. (a) Cell viability on HCT116 cells after 0–40 μmol/L AH-treated with or without 690 nm laser irradiation (0.8 W/cm^2) for 20 min ($n=3$). (b) Fluorescence images of co-stained AM and PI on HCT116 cells after 30 μmol/L AH-treated with or without 690 nm laser irradiation for 20 min. Scale bar: 500 μm. (c) Apoptosis situation on HCT116 cells after 30 μmol/L AH-treated with or without 690 nm laser irradiation for 20 min and quantitative diagrams of apoptotic ($n=3$). (d) ROS testing on HCT116 cells after 30 μmol/L AH-treated with or without 690 nm laser irradiation for 20 min ($n=3$). (e) *In vivo* experiments were conducted on mice following the formation of tumors *via* intraperitoneal drug injection and laser irradiation. Laser treatment of the tumor site was initiated 6–8 h after drug injection and continued every other day. The growth of tumors in mice was observed on the 15th day. (f) Pictures of dissected tumors of the various groups in the nude mice. (g) The following data presents the tumor volumes on the 5th, 10th and 15th day for each group. Tumor dimensions (long and short axes, L and W, respectively) were measured and calculated using the formula $V = L \times W^2/2$. The replicates ($n=4$ or 5) were set up for each group in the tumor size as Fig. 5f. (h) The weight of the dissected tumor groups was determined using an electronic balance ($n=4$ or 5). Data are presented as mean ± standard deviation (SD). $^{**}P < 0.01$, $^{***}P < 0.001$. The comparisons between groups were performed using one-way ANOVA.

death by promoting ROS generation and heat. This strategy may represent a promising therapeutic approach for enhancing cancer cell elimination through ROS/heat-mediated pathways. These findings suggest that our work offers a robust design strategy of the orthogonal molecule in aza-BODIPY system for phototherapy agents.

Using 2,6-dibromo DB-BDP as the starting material, we performed a Suzuki coupling reaction to introduce mono-anthryl moiety to aza-BODIPYs AB-BDP and AH-BDP. AB-BDP and AH-BDP were confirmed by X-ray analysis. We found that the steric bulk of the anthryl group was forced to adopt a *pseudo*-orthogonal structure, avoiding the stereo repulsion. The dihedral angles between the anthryl group and the nucleus were 70.6° for AH-BDP and 87.8° for BA-BDP, respectively. Due to the orthogonal structure enhancing SOCT-ISC, type II ROS ($\Phi_\Delta = 0.15$) is generated by AH-BDP with irradiation, compared to that ($\Phi_\Delta = 0.02$) of aza-BDOPY without anthryl group DH-BDP. The calculated ΔE_{st} for AH-BDP is 0.757 eV, significantly smaller than that of the aza-BDOPY without anthryl group DH-BDP (1.052 eV), which suggested that AH-BDP could possess higher ISC efficiency and thus generate ROS more efficiently, in agreement with the experimental results. Furthermore, AH-BDP NPs had also a good photothermal conversion effect. Self-assembly AH-BDP NPs can efficiently induce HCT116 cells elimination in nude mice through ROS/heat-mediated pathways. The findings of this study suggest that our work offers a robust design strategy of the orthogonal molecule in aza-BODIPY system for phototherapy agents.

Declaration of competing interest

The authors declare that they have no known competing financial interests or personal relationships that could have appeared to influence the work reported in this paper.

CRediT authorship contribution statement

Shu Lv: Methodology, Investigation, Data curation. **Xiuyan Gong:** Methodology, Data curation. **Yunsheng Xue:** Software. **Gaowu Qin:** Writing – review & editing. **Xin-Dong Jiang:** Writing – review & editing, Supervision. **Guiling Wang:** Writing – review & editing.

Acknowledgments

This work was supported by the National Natural Science Foundation of China (Nos. 22078201, U1908202), Liaoning & Shenyang Key Laboratory of Functional Dye and Pigment (Nos. 2021JH13/10200018, 21-104-0-23). We also thank Prof. Yohsuke Yamamoto (Hiroshima University) for his help.

Supplementary materials

Supplementary material associated with this article can be found, in the online version, at doi:10.1016/j.cclet.2025.111171.

References

[1] B. Nasseri, E. Alizadeh, F. Bani, et al., Appl. Phys. Rev. 9 (2022) 011317.
[2] L. Wang, X. Qu, Y. Zhao, et al., ACS Appl. Mater. Interfaces 11 (2019) 35228–35237.
[3] Y. Wang, S. Luo, Y. Wu, et al., ACS Nano 14 (2020) 17046–17062.
[4] T. Dou, F. Xu, X. Xu, et al., Chem. Sci. 12 (2021) 11089–11097.
[5] G. Feng, Q. Zhang, D. Ding, et al., Chem. Soc. Rev. 49 (2020) 8179–8234.
[6] P. Jiang, F. Hu, C. Shen, et al., ACS Appl. Mater. Interfaces 6 (2014) 18008–18017.
[7] D. Zheng, X. He, X. Li, et al., Coord. Chem. Rev. 426 (2021) 213548.
[8] D. Chen, H. Dai, W. Wang, et al., Adv. Sci. 9 (2022) e2200128.
[9] Y. Wang, S. Xu, L. Shi, et al., Angew. Chem. Int. Ed. 60 (2021) 14945–14953.
[10] J. Xie, Y. Wang, W. Choi, et al., Chem. Soc. Rev. 50 (2021) 9152–9201.
[11] Y. Liu, W. Bu, C. Cheng, et al., Angew. Chem. 127 (2015) 8223–8227.
[12] M. Kaur, A. Janaagal, N. Balsukuri, et al., Coord. Chem. Rev. 498 (2024) 215428.
[13] H. Lu, J. Mack, Y. Yang, et al., Chem. Soc. Rev. 43 (2014) 4778–4823.
[14] J. Wang, C. Yu, E. Hao, et al., Coord. Chem. Rev. 470 (2022) 214709.
[15] M. Oyelowo, J. Schaffner, T. Jeaydi, et al., Inorg. Chem. 63 (2024) 24008–24021.
[16] T. Zhang, C. Ma, T. Sun, et al., Coord. Chem. Rev. 390 (2019) 76–85.
[17] Z. Cui, D. Zhang, Y. Huang, et al., Chin. Chem. Lett. 36 (2025) 110460.
[18] M. Gao, Z. Cui, Y. Shen, et al., Chin. Chem. Lett. 36 (2025) 110098.
[19] L. Cao, Y. Li, D. Zhang, et al., Chin. Chem. Lett. 35 (2024) 109735.
[20] A.M. Durantini, L.E. Greene, R. Lincoln, et al., J. Am. Chem. Soc. 138 (2016) 1215–1225.
[21] M. Lan, S. Zhao, W. Liu, et al., Adv. Healthc. Mater. 8 (2019) e1900132.
[22] S. Monro, K.L. Colón, H. Yin, et al., Chem. Rev. 119 (2018) 797–828.
[23] J. Zhao, K. Xu, W. Yang, et al., Chem. Soc. Rev. 44 (2015) 8904–8939.
[24] F. Hu, S. Xu, B. Liu, et al., Adv. Mater. 30 (2018) e1801350.
[25] A. Kamkaew, S.H. Lim, H.B. Lee, et al., Chem. Soc. Rev. 42 (2013) 77–88.
[26] D. Xi, N. Xu, X. Xia, et al., Adv. Mater. 34 (2021) e2106797.
[27] V.N. Nguyen, J. Ha, C.W. Koh, et al., Chem. Mater. 33 (2021) 7889–7896.
[28] V.N. Nguyen, Y. Yan, J. Zhao, et al., Acc. Chem. Res. 54 (2020) 207–220.
[29] A. Atilgan, Y. Beldjoudi, J. Yu, et al., ACS Appl. Mater. Interfaces 14 (2022) 12596–12605.
[30] H. Liang, M. Lu, Z. Mahmood, et al., Angew. Chem. Int. Ed. 62 (2023) e202312600.

[31] Y.Z. Peng, G.C. Guo, S. Guo, et al., Angew. Chem. Int. Ed. 60 (2021) 22062–22069.
[32] H. van Willigen, G. Jones, M.S. Farahat, et al., J. Phys. Chem. A 100 (1996) 3312–3316.
[33] L. Yang, Y. Liu, W. Liu, et al., Bioorg. Med. Chem. Lett. 25 (2015) 5716–5719.
[34] C. Li, T. Sun, X. Li, et al., ACS Appl. Nano Mater. 5 (2022) 18691–18696.
[35] Y. Zhu, J. Liu, M. Lv, et al., Chin. Chem. Lett. 35 (2024) 109446.
[36] A. Gorman, J. Killoran, C. O'Shea, et al., J. Am. Chem. Soc. 126 (2004) 10619–10631.
[37] D. Pinjari, M. Imran, P. Dad, et al., Chem. Eur. J. 30 (2024) e202303799.
[38] G. Dhangar, J.L. Serrano, C. Schulzke, et al., ACS Omega 2 (2017) 3144–3156.
[39] C. Liu, X. Ji, Z. Yu, et al., J. Med. Chem. 66 (2023) 7205–7220.
[40] Z. Yu, J. Zhou, X. Ji, et al., J. Med. Chem. 63 (2020) 9950–9964.
[41] K. Żamojć, M. Zdrowowicz, P.B. Rudnicki-Velasquez, et al., Free Radic. Res. 51 (2016) 38–46.
[42] Y. Zhu, P. Wu, S. Liu, et al., Angew. Chem. Int. Ed. 62 (2023) e202313166.
[43] Y. Dong, B. Dick, J. Zhao, et al., Org. Lett. 22 (2020) 5535–5539.
[44] L. Cao, Z. Cui, D. Zhang, et al., ACS Mater. Lett. 6 (2024) 4765–4773.
[45] D. Xi, M. Xiao, J. Cao, et al., Adv. Mater. 32 (2020) e1907855.
[46] X. Zhao, M. Sun, X. Cao, et al., Adv. Healthc. Mater. 13 (2024) e2400201.
[47] H. Jung, J. Lee, K. Kim, et al., J. Am. Chem. Soc. 139 (2017) 9972–9978.